

Bistability of electron temperature in atomically thin semiconductors in the presence of exciton photogeneration

A.M. Shentsev^{1,2}

¹*Moscow Institute of Physics and Technology, Dolgoprudny, Russia*

²*L. D. Landau Institute for Theoretical Physics, 142432 Chernogolovka, Russia*

(Dated: March 10, 2026)

We study the dynamic equilibrium between trions and excitons in monolayers of transition metal dichalcogenides in the presence of resident charge carriers and continuous photogeneration of excitons. We show that heating of the system via Drude absorption of low-frequency radiation leads to bistability of the steady-state equilibrium. The first is a low-temperature state, in which almost all resident charge carriers are bound into trions. The second state occurs at high temperatures, where most trions are dissociated; in this regime, the heating is more efficient due to the higher Drude conductivity of unbound charge carriers compared to trions. Switching between these two states occurs on a timescale of tens to hundreds of picoseconds and is accompanied by a jump in various observables such as temperature, current, and the intensity of exciton or trion luminescence.

I. INTRODUCTION

Transition metal dichalcogenide monolayers (TMDC MLs) are direct-bandgap semiconductors [1, 2] whose optical properties are largely determined by various multi-particle Coulomb complexes [3–5] with high binding energies. These include neutral excitons (X) and charged excitons (trions): specifically, three-particle complexes in which an exciton is bound to either an electron from the conduction band (the negative trion, X^-) or a hole from the valence band (the positive trion, X^+). The exciton binding energies in these materials are on the order of hundreds of meV, while the trion binding energies are approximately 20–30 meV, i.e., they are about an order of magnitude smaller [6, 7]. Thus, due to their high stability, it is possible to study these complexes over a wide temperature range [8–13].

The binding energy of trions in two-dimensional (2D) TMDCs falls within the terahertz spectral range—a frequency region that is presently the focus of intense research [14–18]. Recent experimental works [19, 20] have demonstrated the conversion of trions into excitons, as well as the possibility of controlling the ratio of trion to exciton concentration by applying picosecond terahertz pulses. Alternatively, such conversion can occur through heating of the electron gas [21, 22], which leads to trion dissociation via collisions with hot electrons whose energies are on the order of the trion binding energy [23]. This collision-induced trion-to-exciton conversion, also termed impact dissociation, is more efficient at low-frequency radiation due to greater heating of the sample. The reverse process—the relaxation of excitons into trions—is most likely mediated by the emission of an optical phonon into the lattice [24]. Notably, in TMDC MLs, the energy of optical phonons can be very close to the trion binding energy [25]; therefore, this relaxation rate is only weakly dependent on temperature [24], in contrast to the impact dissociation of trions, which increases exponentially with temperature.

In this paper, we investigate nonlinear effects [26–

32] arising from the conversion of excitons to trions in TMDC MLs under continuous exciton photogeneration. We show that the exponential increase in trion dissociation rate with temperature leads to a stepwise change in the ratio of the density of unbound resident charge carriers to the trion density. Combined with the fact that trions (being heavier than free carriers) exhibit lower conductivity and shorter energy relaxation times [33], this effect gives rise to bistability [34] in the system’s steady state when it is heated by an external low-frequency field. The first state is a low-temperature one, in which most of the resident charge carriers are bound to excitons, forming trions. The second is a high-temperature state, in which most trions are dissociated, leading to more efficient heating. Switching between these two states occurs on a timescale of 10–100 ps and is accompanied by abrupt changes in various system observables—such as temperature, electric current, fraction of the absorbed-transmitted external electromagnetic field and the intensity of exciton or trion luminescence—forming a hysteresis loop as the heating power is varied.

The article is organized as follows. In Sec. II, we present the dynamic equations for the components of the electron gas and determine the dependence of their equilibrium densities on temperature. The differences between the absorption and cooling rate of trions and resident charge carriers are considered in Sec. III. In Sec. IV, we demonstrate the emergence of bistability in the steady state and the formation of a hysteresis loop for the system’s observables. Here we also consider the influence of system parameters on the bifurcation region. The case of low resident charge carrier densities, as well as the process of temporal relaxation during switching between regimes, is presented in Sec. IV A and IV B, respectively. The main results and conclusions are presented in Sec. V.

II. DYNAMIC EQUATIONS OF THE SYSTEM

We consider n -doped TMDC MLs, with an resident electron density of $n_c = 10^{11} \dots 10^{12} \text{ cm}^{-2}$ in the conduction band. While the type of resident charge carrier is not crucial (and the case of p -doping with holes in the valence band is analogous to our consideration) we focus here on the n -doping scenario. Following the photogeneration of an exciton density n_X , their energy relaxation by optical phonons leads to the formation of X^- trions, whose density we denote as n_T . At the considered resident charge carrier densities, the Fermi energy is much smaller than the trion binding energy, ensuring that the trions remain stable.

For efficient heating of the electron gas, we propose using a low-frequency or static electromagnetic field satisfying $\omega\tau_{tr} \ll 1$, where τ_{tr} is the momentum relaxation time, of resident electrons, see below. Hereafter, it is assumed that $\hbar\omega \ll E_T$ and that the direct exciton-trion transition via photon absorption does not occur. In addition, the temperature is assumed to be much lower than the exciton binding energy, so thermal dissociation of excitons can be neglected. Thus, the dynamic equations for the components of the system are as follows:

$$\frac{dn_e}{dt} = -\gamma n_e n_X + \frac{n_T}{\tau_T} + \beta n_e n_T, \quad (1a)$$

$$\frac{dn_X}{dt} = G_X - \gamma n_e n_X - \frac{n_X}{\tau_X} + \beta n_e n_T, \quad (1b)$$

$$\frac{dn_T}{dt} = \gamma n_e n_X - \frac{n_T}{\tau_T} - \beta n_e n_T, \quad (1c)$$

$$C \frac{dT}{dt} = Q - Q_l. \quad (1d)$$

Here n_e denotes the density of electrons not bound into trions, G_X , see Fig. 1(d), is the rate of photogeneration of the exciton density, T is the temperature of electron gas—assumed, for simplicity, to be common to all components—and C is the heat capacity of the electron gas per unit area, τ_X, τ_T , see Fig. 1(b, d), are lifetimes of exciton and trion, respectively. Q is the Drude absorption power density, Q_l is the energy loss rate density by electron gas. The process with rate $\gamma n_e n_X$, depicted in Fig. 1(c), represents the pairing of excitons and electrons into trions, most likely due to the emission of optical phonons [24]. The term $\beta n_e n_T$, shown in Fig. 1(a), describes the impact dissociation of trions [23], where $\beta(T) \sim \exp(-E_T/k_B T)$ is exponentially activated with increasing temperature, as dissociation occurs via collisions with particles whose energy is on the order of the trion binding energy.

The densities of all components of the system (1) are related by simple linear expressions:

$$n_e + n_T = n_c, \quad (2a)$$

$$\frac{n_X}{\tau_X} + \frac{n_T}{\tau_T} = G_X, \quad (2b)$$

where the first equation corresponds to the conservation of resident charge carriers in the conduction band, and

the second connects the equilibrium densities of excitons n_X and trions n_T to the rate of exciton photogeneration G_X . In the steady state, the rate of electron binding into trions is compensated by impact dissociation and radiative decay of trions

$$\gamma n_X n_e = \beta n_T n_e + \frac{n_T}{\tau_T}. \quad (3)$$

Thus, a stationary point, see Fig. 1, for Eqs. (1) at a given temperature is found by solving a quadratic equation obtained from the Eqs. (2) and (3)

$$\left(\beta + \gamma \frac{\tau_X}{\tau_T} \right) n_e^2 + \left(\gamma \tau_X \left(G_X - \frac{n_c}{\tau_T} \right) + \frac{1}{\tau_T} - \beta n_c \right) n_e - \frac{n_c}{\tau_T} = 0, \quad (4)$$

that has only one root at $n_e, n_T, n_X > 0$. As can be seen in Fig. 1(f), the temperature dependence of the densities of free electrons n_e (blue solid line) and trions n_T (orange solid line) exhibits a stepwise shape. At temperatures below approximately 40 K, almost all charge carriers bind with excitons to form trions. With a further increase in temperature, a sharp rise in the impact dissociation of trions occurs, and the equilibrium concentration of trions rapidly decreases to zero.

It is interesting to compare calculated from Eqs. (1) steady-state concentrations with those predicted by the Saha equation:

$$\frac{n_e n_X}{n_T} = \frac{M_e M_X}{M_T} \times \frac{k_B T}{\pi \hbar^2} e^{-\frac{E_T}{k_B T}}, \quad (5)$$

where M_e, M_X , and M_T are the masses of the electron, exciton, and trion, respectively. In addition to the fact that our system is not in thermodynamic equilibrium, the Saha equation Eq. (5), the solution of which is represented by the dashed lines in Fig. 1(f), does not take into account the photogeneration and radiative recombination of excitons and trions. While the solutions of Eq. (4) and Eq. (5) are qualitatively similar, their differences related to the, strictly speaking, non-equilibrium nature of Eqs. (1) vs. equilibrium Eq. (5) are clearly visible in Fig. 1(f).

The approach used to solve Eq. (4) allows the coefficients of system (1) to be temperature-dependent [24, 35] but does not account for Fermi or Bose correlations between particles. This is insignificant at the low concentrations ($\lesssim 10^{12} \text{ cm}^{-2}$) considered here. At higher particle densities, such correlations can introduce a dependence of the coefficients on the concentration of the system components, meaning that Eq. (4) would no longer have such a simple solution. On the other hand, one can expect that such a sharp change in equilibrium concentrations, shown in Fig. 1(f), will also occur in this case.

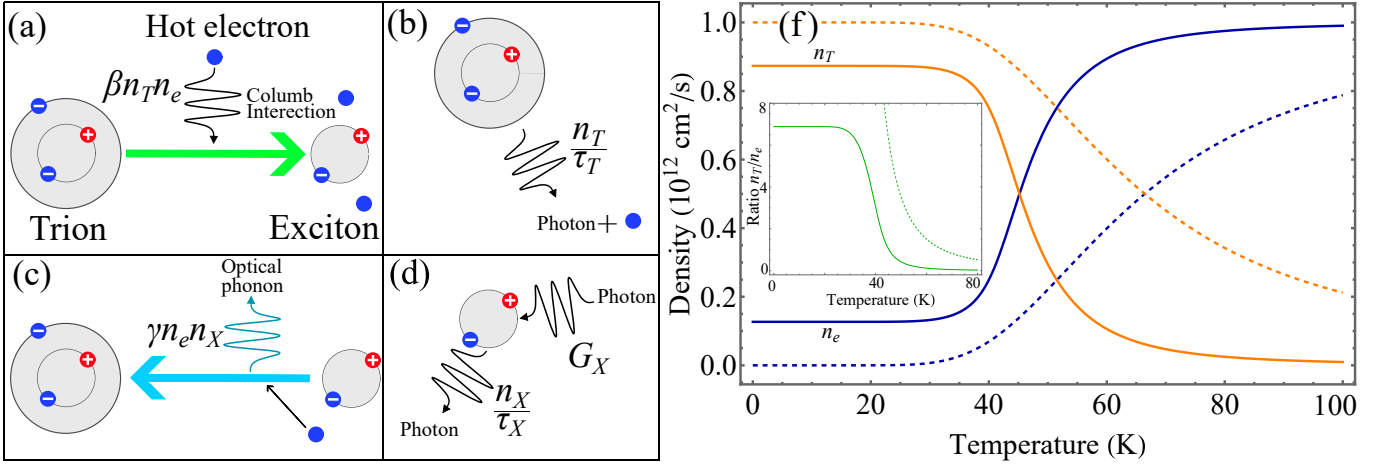


Figure 1. Diagram of the processes described by Eq. (1): (a) Impact trion dissociation with the rate $\beta n_T n_e$ caused by electrons with an energy on the order of E_T ; (b) Radiative recombination of an exciton within a trion (n_T/τ_T), during which an optical photon is emitted and the outer electron remains in the conduction band; (c) Exciton energy relaxation via electron capture from the conduction band, accompanied by optical phonon emission ($\gamma n_e n_X$); (d) Exciton photogeneration G_X and radiative recombination (n_X/τ_X), see text for details. (f) The dependence of the density of unbound electrons n_e and trion density n_T on the temperature of the electron gas. The solid lines correspond to the solution of Eq. (4), while the dashed lines correspond to the Saha equation Eq. (5). Inset shows dependence of ratio n_T/n_e on the temperature of the electron gas. The parameters of calculation are $G_X = 4.5 \cdot 10^{10} \text{ cm}^{-2} \text{ ps}^{-1}$, $\gamma = 0.1 \text{ cm}^2 \text{ s}^{-1}$, $n_c = 10^{12} \text{ cm}^{-2}$, $\tau_X = \tau_T = 50 \text{ ps}$, $\beta = w_0 \frac{k_B T}{E_T} e^{-\frac{E_T}{k_B T}}$, with $w_0 = 1.16 \cdot 10^3 \text{ cm}^2 \text{ s}^{-1}$, $E_T = 25 \text{ meV}$ [19, 23, 24].

III. HEATING AND COOLING OF ELECTRONS AND TRIONS

Within the quasiparticle approach, the low-frequency electric current density ($\omega\tau_{tr} \ll 1$) consists of contributions from free electrons and trions:

$$j = E \times \left(\frac{e^2 n_e \tau_{e,tr}}{M_e} + \frac{e^2 n_T \tau_{T,tr}}{M_T} \right), \quad (6)$$

where $E^2 = \frac{4\pi}{c} I$ is the root mean square field strength in the sample when irradiated with an electromagnetic field of intensity I , and e is the charge of an electron. Consequently, the Drude absorption power density Q is therefore likewise composed of two contributions

$$Q = E \times j = Q_e + Q_T, \quad (7a)$$

$$Q_e = E^2 \times \frac{e^2 n_e \tau_{e,tr}}{M_e}, \quad (7b)$$

$$Q_T = E^2 \times \frac{e^2 n_T \tau_{T,tr}}{M_T}. \quad (7c)$$

In the case of scattering by point defects, the momentum relaxation time is $\tau_{i,tr}^{-1} = nu_i^2 M_i / \hbar^3$, where n is the defects density and u_i is the effective strength of the defects' potential. Here and below, subscript $i = e, T$ denotes electrons and trions, respectively. Taking this into account, the ratio of the absorption power of electrons and trions, r_D , has the form

$$r_D^{-1} = \frac{Q_e/n_e}{Q_T/n_T} = \left(\frac{M_T u_T}{M_e u_e} \right)^2 \sim 10, \quad (8)$$

where we consider $M_T \approx 3M_e$ and $u_T \approx u_e$. In the case the system is heated by a low-frequency field ($\omega\tau_{tr} \ll 1$), the role of longitudinal acoustic and optical phonons in Drude absorption is reduced to a renormalization of the momentum relaxation time τ_{tr} . For simplicity, we neglect these effects; the role of phonons in energy relaxation will be discussed below.

The kinetic energy loss rate Q_l of the electron gas consists of the following components:

$$Q_l = Q_{LA} + Q_O + Q_I. \quad (9)$$

Here Q_{LA} is relaxation via longitudinal long-wave acoustic phonons, Q_O is the relaxation via optical phonons, and Q_I denotes the energy loss due to trion impact dissociation. Given that the optical phonon energy in TMDC MLs is approximately equal to the trion binding energy E_T [24], we neglect any temperature change due to the process of trion formation (characterized by the rate $\gamma n_e n_X$).

The energy relaxation rate via longitudinal acoustic phonons, Q_{LA} , is given by

$$Q_{LA} = \left(\frac{n_e}{\tau_{e,LA}} + \frac{n_X}{\tau_{X,LA}} + \frac{n_T}{\tau_{T,LA}} \right) k_B (T - T_l). \quad (10)$$

Here T_l is the lattice temperature and $\tau_{i,LA}^{-1} = 2M_i^2 |\Xi_i|^2 / \rho \hbar^3$ is a time of energetic relaxation, where Ξ_i is the deformation potential and ρ is the two-dimensional mass density of the crystal. Thus, the energy relaxation rate due to acoustic phonons for trions and electrons is

related as follows:

$$r_{LA} = \frac{Q_{T,LA}/n_T}{Q_{e,LA}/n_e} = \left(\frac{M_T \Xi_T}{M_e \Xi_e} \right)^2 \sim 10, \quad (11)$$

where we also assume that $\Xi_T \approx \Xi_e$. In general, the ratio of the corresponding constants for electrons and trions—such as u , Ξ , and so on—depends on the material [24, 37–39]. Therefore, the difference in absorption r_D and cooling r_{LA} between electrons and trions can be either greater or smaller.

At electron gas temperatures of about 50 K and above, cooling via optical phonons Q_O becomes significant [21, 36]. The corresponding energy relaxation rate is given by

$$Q_O = \left(n_e |D_e^{(0)}|^2 M_e + n_X |D_X^{(0)}|^2 M_X + n_T |D_T^{(0)}|^2 M_T \right) \times \frac{e^{-\frac{\hbar\omega_O}{k_B T}}}{2\rho\hbar}, \quad (12)$$

where $D_i^{(0)}$ is the deformation potential responsible for the interaction of the corresponding particle with optical phonons. This expression is valid specifically for interactions with a homopolar (HP) optical phonon; however, the essential exponential dependence also holds in the general case.

The energy loss due to trion impact dissociation is described by

$$Q_I = E_T \times \beta(T) n_e n_T. \quad (13)$$

Although the total energy of the electron gas is conserved in this process, the trion binding energy E_T is subsequently transferred to the lattice via optical phonon emission $\hbar\omega_O$. Furthermore, since in the Boltzmann limit the system energy is CT , where $C = k_B(n_e + n_X + n_T)$, the left-hand side of Eq. (1d) must contain a term of the form $\frac{dC}{dT}T$, related to the temperature change due to energy sharing between particles. We neglect this term since it scales as $\sim k_B T \times \beta(T) n_e n_T$ and provides only a correction to Eq. (13) of order no larger than $k_B T/E_T$.

Thus, from Eqs. (8) and (11) it is evident that the rates of absorption and cooling due to electrons and trions can differ by an order of magnitude, as a consequence of the large trion effective mass $M_T \approx 3M_e$. Thus, the conductivity of the system, as well as its absorption and cooling characteristics, strongly depend on the ratio between free electrons and trions and can therefore be used to characterize the state of the system. As will be shown below, this can lead to significant instability of the system upon variation of the heating intensity and to the coexistence of two steady states.

IV. BISTABILITY OF THE SYSTEM UNDER HEATING

The relation between the steady-state intensity intensity $I = \frac{c}{4\pi} E^2$ as a function of electron gas temperature T

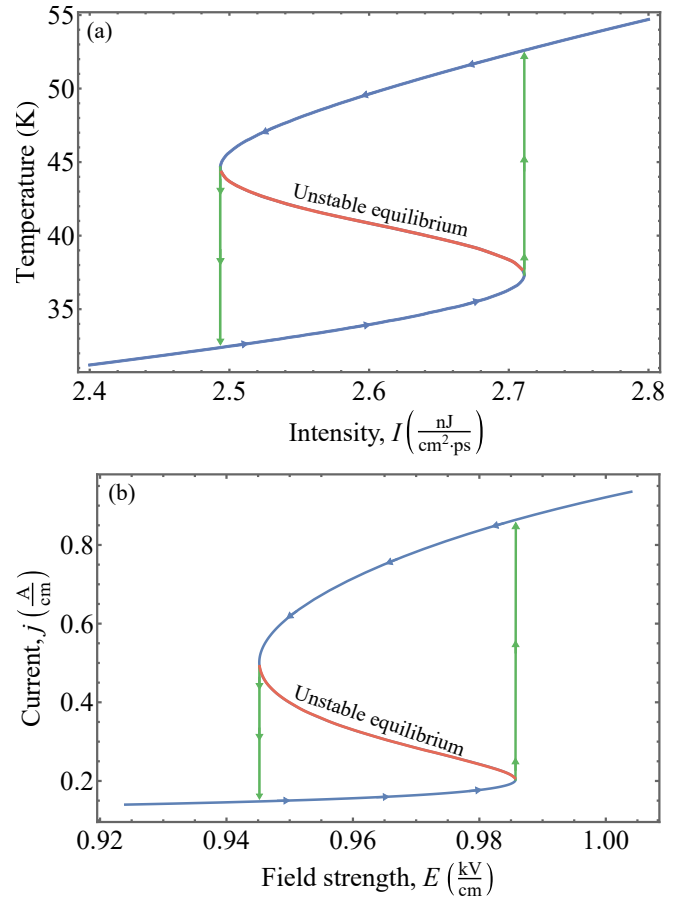


Figure 2. (a) Dependence of electron gas temperature on the heating intensity I . (b) Dependence of electric current density j on the applied electromagnetic field strength E in the sample. Arrows indicate the direction of traversal on the hysteresis loop. The parameters of calculation are $\tau_{e,tr} = 2$ ps, $\tau_{e,LA} = 30$ ps, $r_D = 0$, $r_{LA} = 10$, $D_e^{(0)} = D_h^{(0)} = D_T^{(0)} = 5.2 \cdot 10^8$ eV·cm $^{-1}$, $D_X^{(0)} = 0$, $\rho = 4.46 \cdot 10^{-7}$ g·cm $^{-2}$, $E_T = 25$ meV, $\hbar\omega_O = 30.3$ meV [24], other parameters are the same as ones used for the calculations for Fig. 1.

and the exciton photogeneration rate G_X is obtained by equating absorption power (7) to the energy loss rate (9)

$$I(T, G_X) = \frac{Q_I(n_e, n_X, n_T, T)}{\frac{4\pi}{c} \frac{e^2 \tau_{e,tr}}{M_e} (n_e + r_D n_T)}, \quad (14)$$

where n_e, n_X, n_T are determined from Eqs. (4) and (2). As shown in the inset of Fig. 1, the density ratio n_T/n_e exhibits a step-like dependence. Given the difference in absorption and cooling capacity between trions and electrons, this can result in a non-monotonic dependence of the intensity $I(T, G_X)$ on the electron gas temperature T . Thus, for a certain range of intensities I or field strengths E , the stationary solution bifurcates into two stable branches and one unstable branch, see Fig. 2. The lower and upper branches correspond to the low-temperature and high-temperature plateaus in Fig. 1, respectively. States below the unstable curve—the red

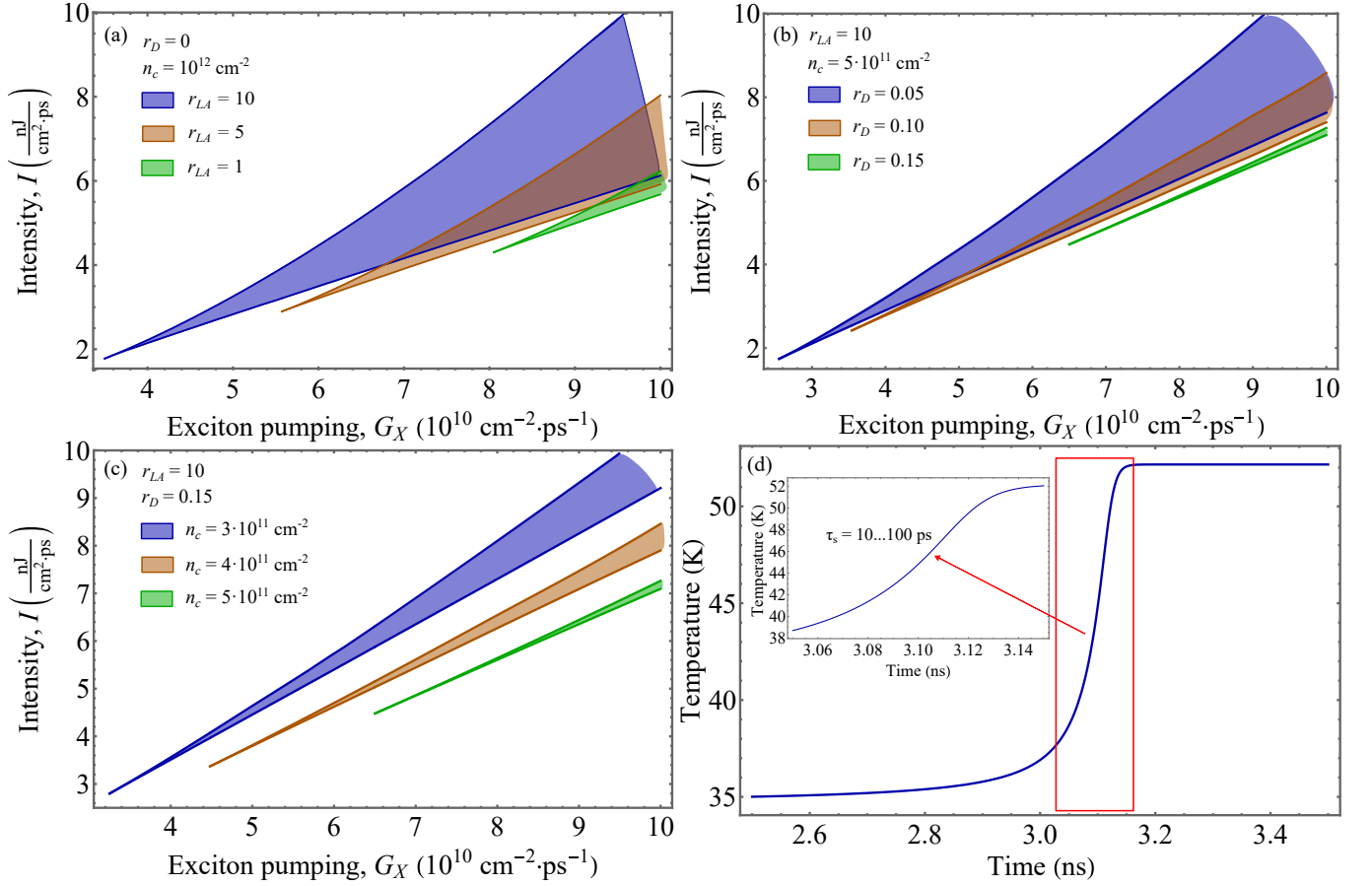


Figure 3. (a) Bifurcation region in the (G_X, I) diagram for different values of r_{LA} , with $r_D = 0$ and $n_c = 10^{12} \text{ cm}^{-2}$. (b) Same for different values r_D , with $r_{LA} = 10$ and $n_c = 5 \cdot 10^{11} \text{ cm}^{-2}$, (c) Same for different values n_c , with $r_D = 0.15$ and $r_{LA} = 10$. (d) Temporal evolution of temperature, corresponding to the right vertical line in Fig. 2, with an initial deviation from equilibrium of 0.1 K. The characteristic switching time is $\tau_s \sim 10 \dots 100 \text{ ps}$.

line in Fig. 2—relax to the low-temperature branch, while those above it relax to the high-temperature branch. The green vertical lines demarcate the boundaries of the hysteresis loop for various system characteristics, including temperature, electric current, the absorbed and transmitted fractions of the external electromagnetic field, and the densities of excitons and trions.

The bifurcation region in the (G_X, I) diagram is highly sensitive to system parameters, as seen in Fig. 3(a–c). It narrows and shifts toward higher values of both the exciton photogeneration rate G_X and the heating intensity I , as shown in Fig. 3(a,b), with decreasing difference in absorption and cooling between trions and electrons described by the parameters r_D and r_{LA} introduced in Eqs. (8) and (11). This is a result of the fact that the loss of kinetic energy during trion impact dissociation $\beta(T)n_e n_T$, sharply increases with temperature, making the $I(T)$ dependence more monotonic. Consequently, as the differences in thermal behavior between resident charge carriers and trions diminish, the bifurcation region shifts toward a larger n_X/n_c ratio, where the contribution of trion impact dissociation to Q_l is less significant,

see Fig. 3(c). In order to get more detailed insight into the physics of bistability we consider below a simplified limiting case where $n_c \ll n_X$.

A. Low electron density regime

As can be seen in Fig. 3(c), the bifurcation effect is more pronounced at low densities of resident charge carriers $n_c \ll n_X$. In this regime, the equilibrium electron density can be written as

$$n_e = \begin{cases} \frac{n_c}{1 + \gamma \tau_T n_X} & \text{at } \beta \ll \gamma n_X / n_c, \\ n_c - \frac{\gamma n_X}{\beta} & \text{at } \beta \gg \gamma n_X / n_c, \end{cases} \quad (15)$$

where we consider the exciton density to be constant, $n_X = G_X \tau_X - \tau_X n_T / \tau_T \approx G_X \tau_X$. The temperature on the lower (L) branch is described by

$$T_L = T_l + E^2 \times \theta_L \left(\frac{1 - r_D}{1 + \gamma \tau_T n_X} + r_D \right), \quad (16)$$

where θ_L is determined by the system parameters

$$\theta_L = \left(\frac{k_B n_X}{\tau_{X,LA}} + \frac{r_{LA} k_B n_c}{\tau_{e,LA}} \times \frac{\gamma \tau_T n_X}{1 + \gamma \tau_T n_X} \right)^{-1} \times \frac{e^2 n_c \tau_{e,tr}}{M_e}. \quad (17)$$

Here we neglect the contribution of impact dissociation Q_I and optical phonons Q_O to cooling on the lower hysteresis branch, since $n_c \ll n_X$ and the deformation potential for excitons $D_X^{(0)} \sim 0.1 D_e^{(0)}$ is small in TMDC MLs [24]. Therefore, its contribution is insignificant at these temperatures. At the same time, we cannot neglect the trion contribution to Q_{LA} , because $r_{LA} n_c$ and n_X can be of the same order for large r_{LA} . If we disregard the optical phonon contribution, then for the upper (U) branch we obtain the following equation

$$T_U = T_l + E^2 \times \theta_U \left(1 - (1 - r_D) \frac{\gamma n_X}{\beta(T_U) n_c} \right), \quad (18)$$

where θ_U has the form

$$\theta_U = \frac{\tau_{X,LA}}{k_B n_X} \times \frac{e^2 n_c \tau_{e,tr}}{M_e}. \quad (19)$$

This approach gives predict the following expression for the temperature difference between the branches: $T_U - T_L \sim \theta_U \times E^2$. In practice, while reducing n_c or increasing n_X diminishes the significance of exponentially activated processes on the lower branch, it thereby shifts T_U to higher temperatures, where these processes remain relevant, see Fig. 4(a). As evident from the Fig. 4, even at $n_X/n_c = 12.5$, cooling via optical phonon Q_O is the dominant process on the upper branch. Note that cooling is primarily via electrons and trions, with the exciton contribution being insignificant at $D_X = 0.1 D_e$. Consequently, the optical phonon contribution (12) must be included in the upper branch analysis, as it largely governs the branch's location. The slowdown in the growth of cooling via acoustic phonons Q_{LA} with increasing temperature is due to a decrease in the proportion of trions, whose energy relaxation occurs faster than that of free electrons. Meanwhile, the impact dissociation term Q_I , while still appreciable at this n_c , diminishes as the resident charge carrier density n_c further decreases, since this process scales as $Q_I \sim n_c^2$.

B. Switching time

The switching process corresponding to the green vertical lines in Fig. 2 (and dashed green lines in Fig. 4(a)) involves changes in both temperature and the electron-to-trion density ratio. Here by switching time we refer to the characteristic time in significant non-equilibrium, rather than the characteristic time of exiting or establishing equilibrium, which determines the tails in Fig. 3(d),

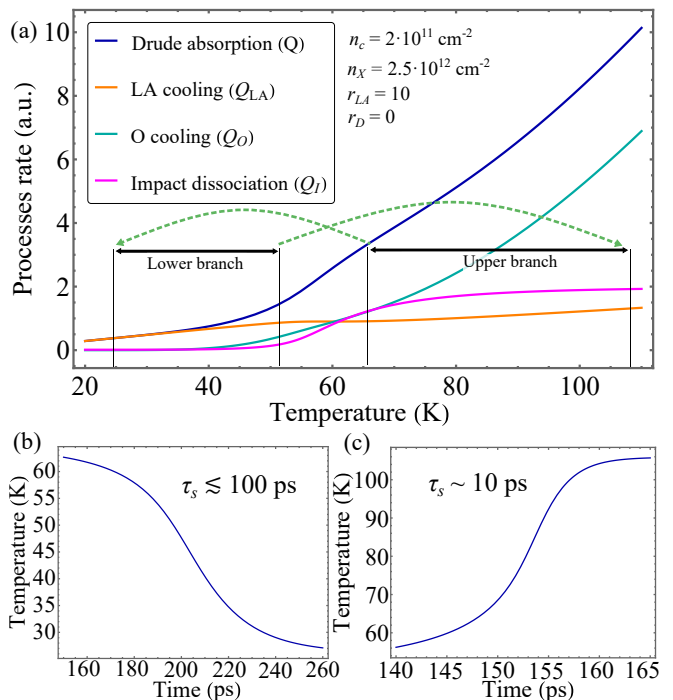


Figure 4. (a) Dependence of the thermal process power (a.u.) on electron gas temperature (K). Black arrows illustrate the temperature ranges where bistability exists. Green dashed lines correspond to switching between branches at the boundaries of the hysteresis loop, as indicated by the green vertical lines in Fig. 2. (b) Temporal evolution of temperature corresponding to the left green dotted arrow from (a), namely, to the switching process with decreasing temperature. The characteristic switching time is $\tau_s \lesssim 100 \text{ ps}$. (c) Temporal evolution of temperature corresponding to the right green dotted arrow from (a), i.e., to the switching process with increasing temperature. The characteristic switching time is $\tau_s \sim 10 \text{ ps}$, which is considerably shorter than that in (b). The parameters of calculation are $n_c = 2 \cdot 10^{11} \text{ cm}^{-2}$, $G_X = 5 \cdot 10^{10} \text{ cm}^{-2} \text{ ps}^{-1}$, $r_{LA} = 10$, $r_D = 0$, initial deviation of temperature from equilibrium for (b,c) is $\Delta T \lesssim 1 \text{ K}$, $D_X^{(0)} = 5.2 \cdot 10^7 \text{ eV} \cdot \text{cm}^{-1}$, other parameters are the same as ones used for the calculations for Fig. 1 and Fig. 2.

which will be discussed later. For $n_X \sim n_c \sim 10^{12} \text{ cm}^{-2}$, the characteristic switching time τ_s is on the order of tens to hundreds of picoseconds, as shown in Fig. 3(d). One can naively separate the switching process into conversion and heating processes. The characteristic time of conversion processes τ_C can be expressed as the inverse of the transition rate per electron

$$\tau_C \sim \frac{1}{\gamma n_X} \sim \frac{1}{\beta n_T}. \quad (20)$$

Here, the rate of trion formation γn_X is of the same order of magnitude as the impact dissociation rate βn_T . This follows from the fact that the radiative term in Eq. (3), normalized to the concentration of unpaired electrons n_e , has the form $\frac{1}{\tau_T} \frac{n_T}{n_e}$ and decreases rapidly over almost the entire temperature range under consideration, as shown

in the inset of Fig. 1(f), except near the onset of the lower branch. With increasing exciton density, the characteristic conversion time decreases, which can be attributed to enhanced nonlinear terms that lead to faster dynamics in the system. The characteristic heating time τ_H is

$$\tau_H \sim \frac{k_B(n_c + n_X) \times (T_U - T_L)}{\frac{4\pi}{c} I \times \frac{n_c e^2 \tau_{e,tr}}{M_e}}, \quad (21)$$

where, for this estimate, the heat capacity is calculated in the Boltzmann limit. In the limit $n_c \ll n_X$, the switching dynamics are asymmetric, as shown in Fig. 4(b,c): Switching with increasing temperature, i.e., from the lower temperature to the higher temperature state, occurs notably faster ($\tau_s \sim 10$ ps) than with decreasing temperature ($\tau_s \lesssim 100$ ps). For $T_U - T_L$ from the preceding section, Eq. (21) reduces to the simple form $\tau_H \sim \tau_{X,LA} \sim 50$ ps. The asymmetry arises because including cooling via optical phonons in Eq. (18)—as discussed in Sec. IV A—significantly limits the growth of the temperature difference $T_U - T_L$ corresponding to the switching with increasing temperature (right dashed green line in Fig. 4(a)) and, to a lesser extent, affects switching with decreasing temperature (left dashed green line in Fig. 4(a)). This, in turn, reduces the characteristic thermal switching time τ_H : the system's response rate to temperature changes increases with intensity $I \sim E^2$, while the temperature range $T_U - T_L$ varies only slightly. This decrease occurs asymmetrically, which explains the behavior observed in Fig. 4(b,c). Moreover, since an increase in the exciton density n_X leads to higher intensity, it consequently reduces both τ_H and the overall switching time $\tau_s = \tau_C + \tau_H$.

As for the tails, the departure from equilibrium (left tail in Fig. 3(f)) always occurs more slowly than its subsequent establishment (right tail in Fig. 3(f)). This can be described as follows: Let the temperature evolution over time near the equilibrium temperature be given by

$$\frac{d\Delta T}{dt} = a\Delta T + b(\Delta T)^2, \quad (22)$$

where ΔT denotes the deviation of the temperature from the equilibrium one. Here, a stable equilibrium corresponds to $a < 0$, while an unstable equilibrium corresponds to $a > 0$. Since at the boundaries (green vertical lines) of the hysteresis loop, see Fig. 2, the switching between branches begins at the intersection of stable (blue lines) and unstable (red line) equilibrium, where $a = 0$ (with $b > 0$ for the right boundary and $b < 0$ for the left), it follows that the time to exit equilibrium scales as $\sim (\Delta T)^{-1}$, whereas the time of its subsequent establishment scales as $\sim \ln(\Delta T)$.

V. CONCLUSION

In this work, we have examined the conditions for bistability arising from the strong differences in the absorption and cooling capacities of electrons and trions in

atomically thin TMDCs. It manifests itself as a reduction in the conductivity of the electron gas due to the formation of trions, which are the bound states consisting of an electron and a heavier, weakly field-interacting exciton. This effect, combined with the step-like dependence of the equilibrium electron-to-trion density ratio on temperature, leads to bistability and hysteresis in various system quantities, namely temperature, electric current, fraction of the absorbed-transmitted external electromagnetic field and the intensity of exciton or trion luminescence.

We present an explicit expression for the intensity as a function of electron gas temperature, which can be non-monotonic. This non-monotonicity leads to the emergence of two steady states when the system is heated by an electromagnetic field. The switching time between these two states is on the order of 10...100 ps and increases with increase in the ratio of the exciton density to the resident charge carrier density. Moreover, as the difference in absorption and cooling between trions and electrons decreases, the bistability region narrows and shifts toward a higher exciton photogeneration rate.

In contrast to bulk silicon, where heating by a microwave field with presence exciton photogeneration induces self-oscillations in the density of electrons and holes not bound into excitons [26, 27], such behavior does not occur in the present system.

Thus, our results demonstrate the possibility of bistability upon heating of TMDC MLs under continuous exciton photogeneration.

ACKNOWLEDGMENTS

The author is grateful M. M. Glazov for valuable discussions and acknowledges support of the Ministry of Science and Higher Education of the Russian Federation (project no. FFWR-2024-0017).

- [1] K. F. Mak, C. Lee, J. Hone, J. Shan, and T. F. Heinz, Atomically thin MoS₂: a new direct-gap semiconductor, *Phys. Rev. Lett.* **105**, 136805 (2010).
- [2] A. Splendiani, L. Sun, Y. Zhang, T. Li, J. Kim, C.-Y. Chim, G. Galli, and F. Wang, Emerging photoluminescence in monolayer MoS₂, *Nano Lett.* **10**, 1271 (2010).
- [3] M. V. Durnev and M. M. Glazov, Excitons and trions in two-dimensional semiconductors based on transition metal dichalcogenides, *Phys. Usp.* **61**, 825–845 (2018).
- [4] E. L. Ivchenko, Optical spectroscopy of semiconductor nanostructures (Alpha Science, Harrow, 2005).
- [5] M. A. Semina and R. A. Suris, Localized excitons and trions in semiconductor nanosystems, *Phys. Usp.* **65**, 111 (2022).
- [6] E. Courtade, M. Semina, M. Manca, M. Glazov, C. Robert, F. Cadiz, G. Wang, T. Taniguchi, K. Watanabe, M. Pierre, et al., Charged excitons in monolayer WSe₂: Experiment and theory, *Phys. Rev. B* **96**, 085302 (2017).
- [7] K. F. Mak, K. He, C. Lee, G. H. Lee, J. Hone, T. F. Heinz, and J. Shan, Tightly bound trions in monolayer MoS₂, *Nat. Mater.* **12**, 207 (2013).
- [8] J. Xiao, M. Zhao, Y. Wang, and X. Zhang, Excitons in atomically thin 2D semiconductors and their applications, *Nanophotonics* **6**, 1309 (2017).
- [9] A. Chernikov, T. C. Berkelbach, H. M. Hill, A. Rigosi, Y. Li, B. Aslan, D. R. Reichman, M. S. Hybertsen, and T. F. Heinz, Exciton binding energy and nonhydrogenic rydberg series in monolayer WS₂, *Phys. Rev. Lett.* **113**, 076802 (2014).
- [10] J. S. Ross, S. Wu, H. Yu, N. J. Ghimire, A. M. Jones, G. Aivazian, J. Yan, D. G. Mandrus, D. Xiao, W. Yao, et al., Electrical control of neutral and charged excitons in a monolayer semiconductor, *Nat. Commun.* **4**, 1474 (2013).
- [11] P. Massignan, R. Schmidt, G. E. Astrakharchik, A. İmamoglu, M. Zwierlein, J. J. Arlt, and G. M. Bruun, Polarons in atomic gases and two-dimensional semiconductors, [arXiv:2501.09618](https://arxiv.org/abs/2501.09618) (2025).
- [12] Y. G. Davila, F. W. Silva, M. C. Oliveira, Z. Yu, T. C. Carvalho, C. C. dos Santos, A. G. Souza Filho, M. Terrones, R. S. Alencar, and B. C. Viana, Temperature and power-dependent photoluminescence spectroscopy in suspended WSe₂ monolayer, *J. Phys. D: Appl. Phys.* **57**, 165304 (2024).
- [13] X.-X. Zhang, Y. You, S. Y. F. Zhao, and T. F. Heinz, Experimental evidence for dark excitons in monolayer WSe₂, *Phys. Rev. Lett.* **115**, 257403 (2015).
- [14] S. Ganichev, W. Prettl, and W. Prettl, *Intense Terahertz Excitation of Semiconductors*, Oxford science publications (OUP Oxford, 2006).
- [15] J. Lampin, G. Mouret, S. Dhillon, and J. Mangeney, Thz spectroscopy for fundamental science and applications, *Photoniques* **101**, 33 (2020).
- [16] M. Helm, S. Winnerl, A. Pashkin, J. M. Klopff, J.-C. Deinert, S. Kovalev, P. Evtushenko, U. Lehnert, R. Xiang, A. Arnold, et al., The Elbe infrared and THz facility at Helmholtz-zentrum Dresden-Rossendorf, *Eur. Phys. J. Plus* **138**, 158 (2023).
- [17] Y. Lu, Y. Huang, J. Cheng, R. Ma, X. Xu, Y. Zang, Q. Wu, and J. Xu, Nonlinear optical physics at terahertz frequency, *Nanophotonics* **13**, 3279–3298 (2024).
- [18] S. Leinß, T. Kampftrath, K. v. Volkmann, M. Wolf, J. T. Steiner, M. Kira, S. W. Koch, A. Leitenstorfer, and R. Huber, Terahertz coherent control of optically dark paraexcitons in Cu₂O, *Phys. Rev. Lett.* **101**, 246401 (2008).
- [19] T. Venanzi, M. Cuccu, R. Perea-Causin, X. Sun, S. Brem, D. Erkensten, T. Taniguchi, K. Watanabe, E. Malic, M. Helm, et al., Ultrafast switching of trions in 2D materials by terahertz photons, *Nat. Photonics* **18**, 1344 (2024).
- [20] M. Cuccu, T. Venanzi, E. Wietek, X. Sun, R. Perea-Causin, T. Taniguchi, K. Watanabe, E. Malic, M. Helm, S. Winnerl, et al., Terahertz-induced population transfer between exciton complexes in monolayer WSe₂, *Phys. Rev. B* **112**, 205302 (2025).
- [21] T. Venanzi, M. Selig, S. Winnerl, A. Pashkin, A. Knorr, M. Helm, and H. Schneider, Terahertz-induced energy transfer from hot carriers to trions in a MoSe₂ monolayer, *ACS Photonics* **8**, 2931 (2021).
- [22] G. V. Budkin and S. A. Tarasenko, Heating and cooling of a two-dimensional electron gas by terahertz radiation, *JETP* **112**, 656 (2011).
- [23] A. Shentsev and M. Glazov, Terahertz radiation induced attractive-repulsive fermi polaron conversion in transition metal dichalcogenide monolayers, [arXiv:2509.15708](https://arxiv.org/abs/2509.15708) (2025).
- [24] S. Ayari, S. Jaziri, R. Ferreira, and G. Bastard, Phonon-assisted exciton/trion conversion efficiency in transition metal dichalcogenides, *Phys. Rev. B* **102**, 125410 (2020).
- [25] Z. Jin, X. Li, J. T. Mullen, and K. W. Kim, Intrinsic transport properties of electrons and holes in monolayer transition-metal dichalcogenides, *Phys. Rev. B* **90**, 045422 (2014).
- [26] B. Ashkinadze and A. Subashiev, Self-oscillations in an exciton-electron system with impact ionization of excitons, *JETP Lett.* **46**, 357 (1987).
- [27] B. Ashkinadze, V. Belkov, and A. Subashiev, Optical and electrical bistability induced by exciton ionization processes, *Phys. Status Solidi B* **150**, 533 (1988).
- [28] L. L. Bonilla, M. Carretero, and E. Mompó, Nonlinear charge transport and excitable phenomena in semiconductor superlattices, *Entropy* **26**, 672 (2024).
- [29] K. Mourzidis, V. Jindal, M. Glazov, A. Balocchi, C. Robert, D. Lagarde, P. Renucci, L. Lombez, T. Taniguchi, K. Watanabe, et al., Exciton formation in two-dimensional semiconductors, *Phys. Rev. X* **15**, 031078 (2025).
- [30] R. Braunstein, Nonlinear optical effects, *Phys. Rev.* **125**, 475 (1962).
- [31] A. Genco and G. Cerullo, Optical nonlinearity goes ultrafast in 2D semiconductor-based nanocavities, *Light Sci. Appl.* **11**, 127 (2022).
- [32] S. Wiczorek and W. W. Chow, Bifurcations and chaos in a semiconductor laser with coherent or noisy optical injection, *Opt. Commun.* **282**, 2367 (2009).
- [33] J. Zipfel, K. Wagner, M. A. Semina, J. D. Ziegler, T. Taniguchi, K. Watanabe, M. M. Glazov, and A. Chernikov, Electron recoil effect in electrically tunable MoSe₂ monolayers, *Phys. Rev. B* **105**, 075311 (2022).

- [34] P. Blanchard, R. L. Devaney, and G. R. Hall, Differential equations, Thomson Brooks (2006).
- [35] M. Palummo, M. Bernardi, and J. C. Grossman, Exciton radiative lifetimes in two-dimensional transition metal dichalcogenides, *Nano Lett.* **15**, 2794 (2015).
- [36] K. Kaasbjerg, K. S. Bhargavi, and S. S. Kubakaddi, Hot-electron cooling by acoustic and optical phonons in monolayers of MoS₂ and other transition-metal dichalcogenides, *Phys. Rev. B* **90**, 165436 (2014).
- [37] H. V. Phuc, N. N. Hieu, B. D. Hoi, N. V. Hieu, T. V. Thu, N. M. Hung, V. V. Ilyasov, N. A. Poklonski, and C. V. Nguyen, Tuning the electronic properties, effective mass and carrier mobility of MoS₂ monolayer by strain engineering: first-principle calculations, *J. Electron. Mater.* **47**, 730 (2018).
- [38] K. Zollner, P. E. F. Junior, and J. Fabian, Strain-tunable orbital, spin-orbit, and optical properties of monolayer transition-metal dichalcogenides, *Phys. Rev. B* **100**, 195126 (2019).
- [39] S. Shree, M. Semina, C. Robert, B. Han, T. Amand, A. Balocchi, M. Manca, E. Courtade, X. Marie, T. Taniguchi, et al., Observation of exciton-phonon coupling in MoSe₂ monolayers, *Phys. Rev. B* **98**, 035302 (2018).